Supplementary Information

Lewis Acidic W/WO_{3-x} heterostructure coupled Ir catalysts with low Ir-loading for Efficient pH-Universal Water Splitting

Wenjie Shao[§], Yiming Zhang[§], Rui Yan, Tian Ma, and Shuang Li**

Supplementary Methods

1. Materials and Chemicals

All chemicals were used as received without further purification. Tungsten chloride (WCl_6, 99%, Aladdin), iridium (III) chloride hydrate ($IrCl_3 \cdot xH_2O$, 99%, Energy Chemical), ethanol (CH_3CH_2OH, 99.5%, Aladdin). Ir on Vulcan XC-72 (Ir/C, 20 wt.%, Premetek Company), Pt on Vulcan XC-72 (Pt/C, 20 wt.%, Premetek Company), nafion (D-520, 5% w/w in water and 1-propanol, Energy Chemical), sodium hydroxide (KOH, 85%, Aladdin), concentrated sulfuric acid (H_2SO_4, 95%~98%, XiLong Scientific), sodium phosphate dibasic (Na_2HPO_4, 99%, Aladdin), and sodium dihydrogen phosphate anhydrous ($NaH_2PO_4 \cdot 2H_2O$, 99%, Aladdin). Anion exchange membranes (Fumasep FAA-3-PK-130, 110-130 μm thickness) were purchased from SCI Materials Hub. Deionized water and ultrapure water are made in our laboratory, and all solutions for electrochemical tests are prepared with ultrapure water.

2. Electrochemical Measurements

In a typical preparation of catalyst ink, 10 mg of each catalyst was blended with 1.0 mL Nafion ethanol solution (0.5 wt.%) in an ultrasonic bath for 30 min. The nickel foam (NF) was ultrasonically cleaned by acetone, ethyl alcohol, and ultrapure water in sequence for 20 min. Subsequently, the NF was submerged in 2 M HCl for 20 min, rinsed with ultrapure water several times to remove any additional acid, and then left dry in the air. Then, a fixed volume of catalyst ink (10 mg mL^{-1}) was pipetted onto the glassy carbon electrode with a 5 mm diameter (0.196 cm^2, loading: 0.255 mg cm^{-2}) for HER and OER test in 1.0 M KOH, 0.5 M H_2SO_4, and 1.0 M phosphate-buffered saline (PBS) to evaluate the catalytic activity of various catalysts in different pH.

All the electrochemical performances were evaluated on the Gamry reference 600 workstation (Gamry, USA) with a standard three-electrode system in different electrolytes at room temperature

with automatic iR compensation, in which the 0.5 M H_2SO_4 and 1.0 M KOH electrolyte solutions were prepared from 95~98% H_2SO_4 and KOH pellets with ultrapure water, respectively, the 1.0 M PBS was prepared by diluting a mixture of 0.62 mol Na_2HPO_4 and 0.38 mol NaH_2PO_4 to 1.0 L using ultrapure water (15 MΩ, Milli-Q). A commercial reversible hydrogen electrode (RHE) was used as the reference electrode, and the graphite rod was used as the counter electrode. The Hg/HgO reference electrode (placed in saturated KCl solution that was periodically refreshed to counteract the contamination from electrolytes) calibrated with RHE in 0.5 M H_2SO_4, 1.0 M KOH, or 1.0 M PBS was used as a reference electrode for long-time stability measurement.

Especially for all HER tests, the electrolytes were saturated with Ar (99.99%) by purging Ar into the aqueous solutions for 30 min and then maintaining the flow of Ar throughout all the electrochemical measurements. The HER and OER polarization curves were obtained at a rotating speed of 1600 rpm with a sweep rate of 10 mV s^{-1}, and corrected with real-time iR by Gamry reference 600 potentiostats at a resistance of 4.8 ohms. The water splitting experiment was respectively dropping the Ir-W/WO_{3-x} and Ir-W on NF and carried out in an H-type electrolytic cell separated by an anion-exchange membrane for 1.0 M PBS.

The mass activity is calculated based on the following equation: $\text{mass activity} = \frac{I}{m}$, where I (A) is the measured current. m (mg) is the mass of Ir loaded on a glassy carbon electrode.

The turnover frequency (TOF) is calculated based on the following equation: $\text{TOF} = \frac{I}{\alpha F n}$, where α = 2 for HER and α = 4 for OER. I (A) is the measured current. F is the Faraday constant (96485 C mol^{-1}). n (mol) is the number of active metals of Ir in the catalysts, which was calculated based on the weight content from XPS measurement.

Supplementary Figures and Tables

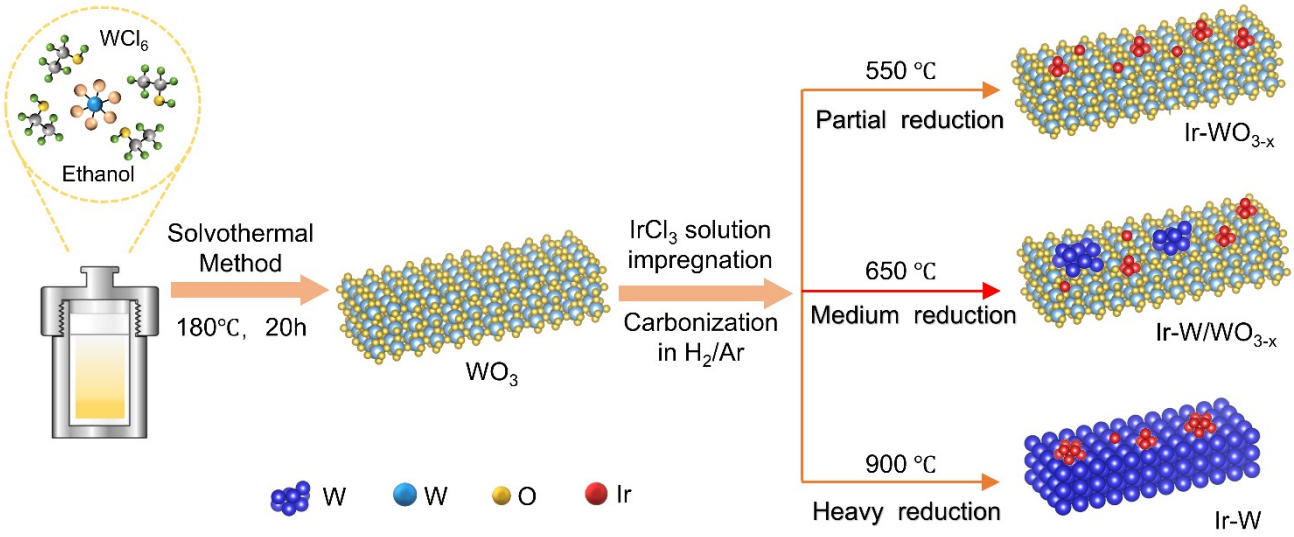

Fig. S1. Schematic illustration of the synthesis process of Ir-WO_{3-x}, Ir-W/WO_{3-x}, and Ir-W.

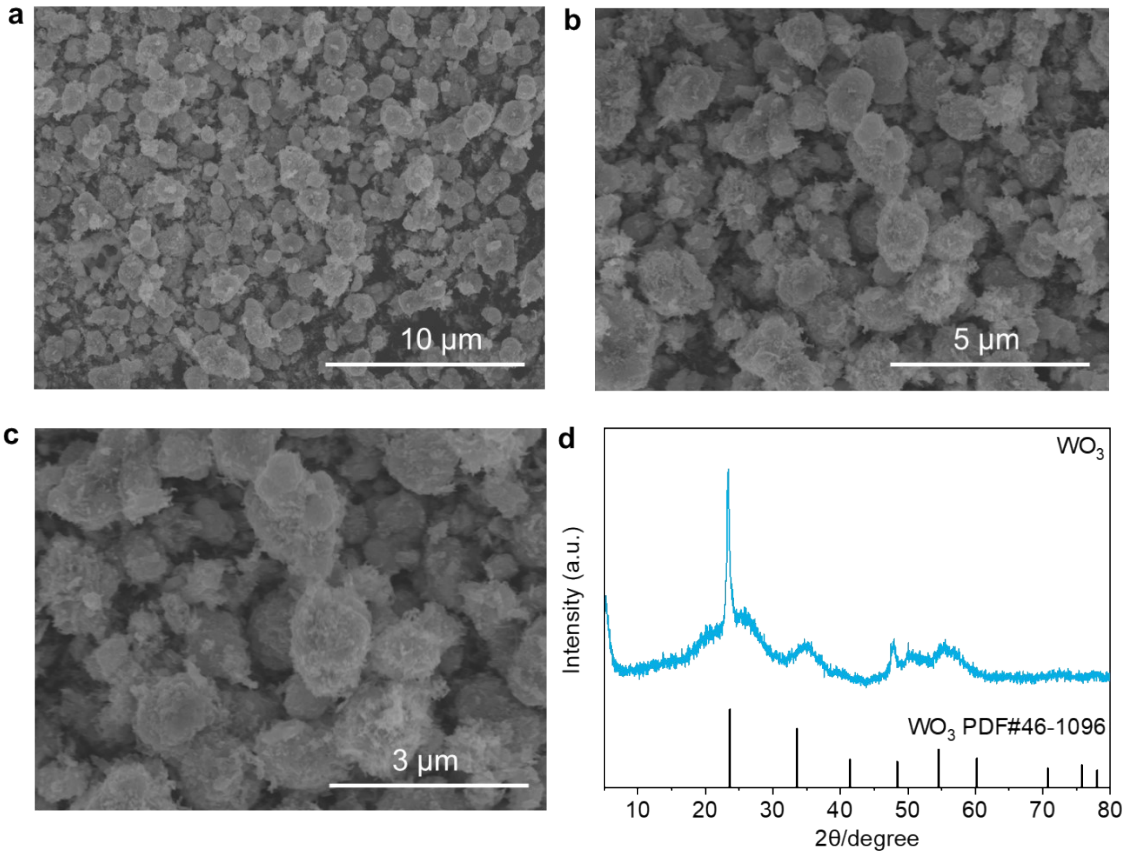

Fig. S2. (a-c) The SEM images of WO_3 at different magnifications. (d) The XRD pattern of WO_3.

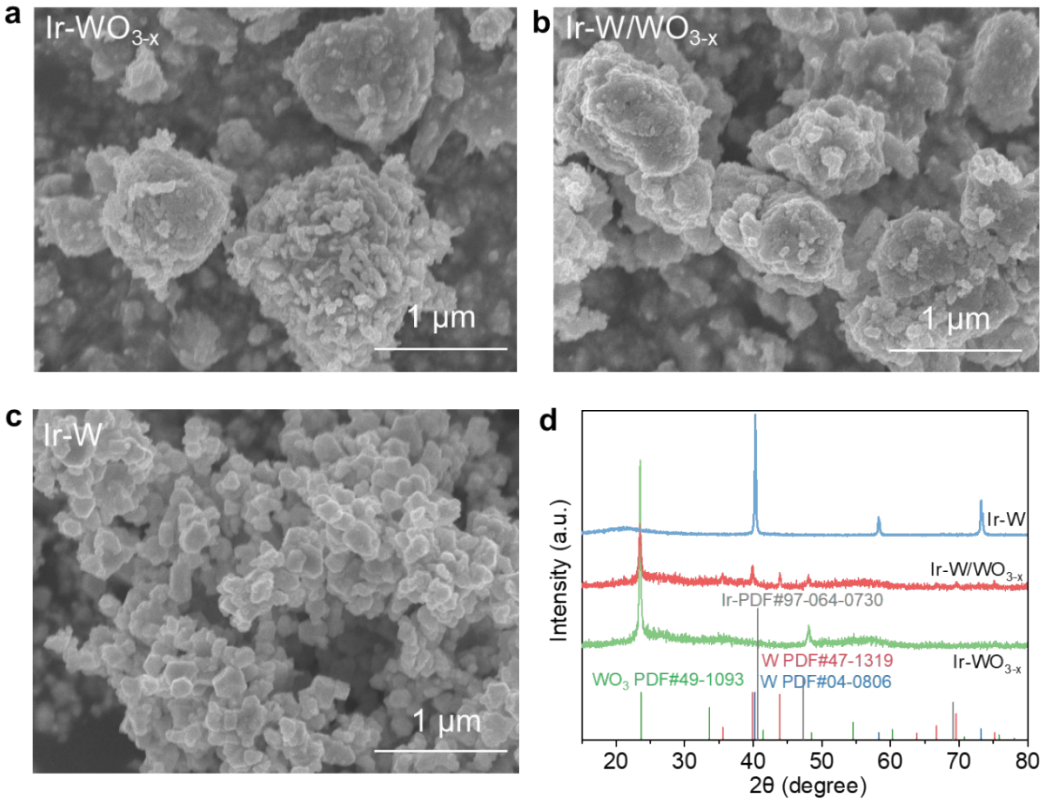

Fig. S3. The SEM image of Ir-WO_{3-x} (a), Ir-W/WO_{3-x} (b), and Ir-W (c), respectively. (d) The XRD patterns of Ir-WO_{3-x}, Ir-W/WO_{3-x}, and Ir-W.

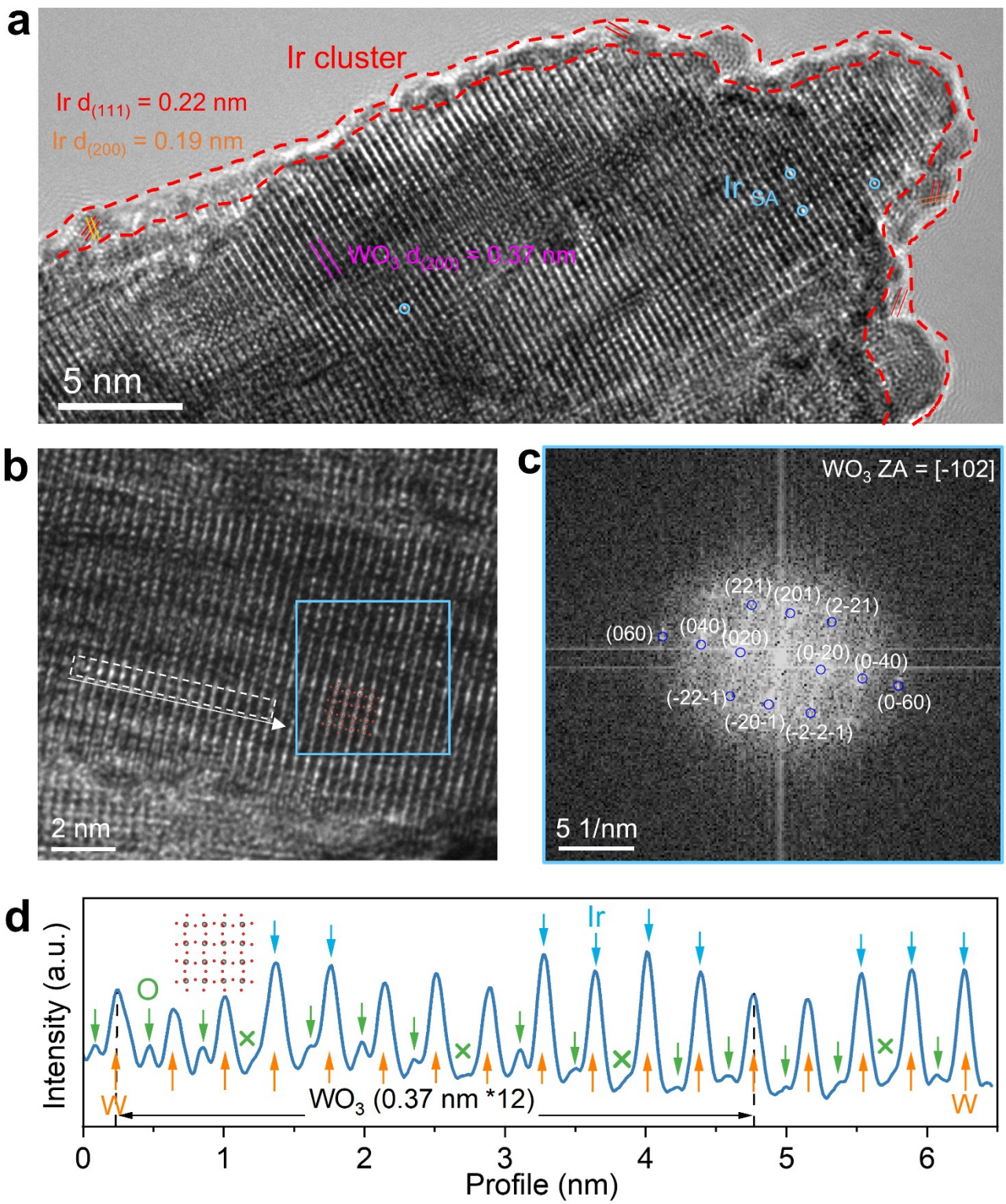

Fig. S4. (a-b) The HRTEM images of Ir-WO_{3-x}, and (c) corresponding FFT pattern along with the [-102] zone axis from the blue box in (b). (d) The line intensity profiles of the white dotted area of Ir-WO_{3-x} from (b).

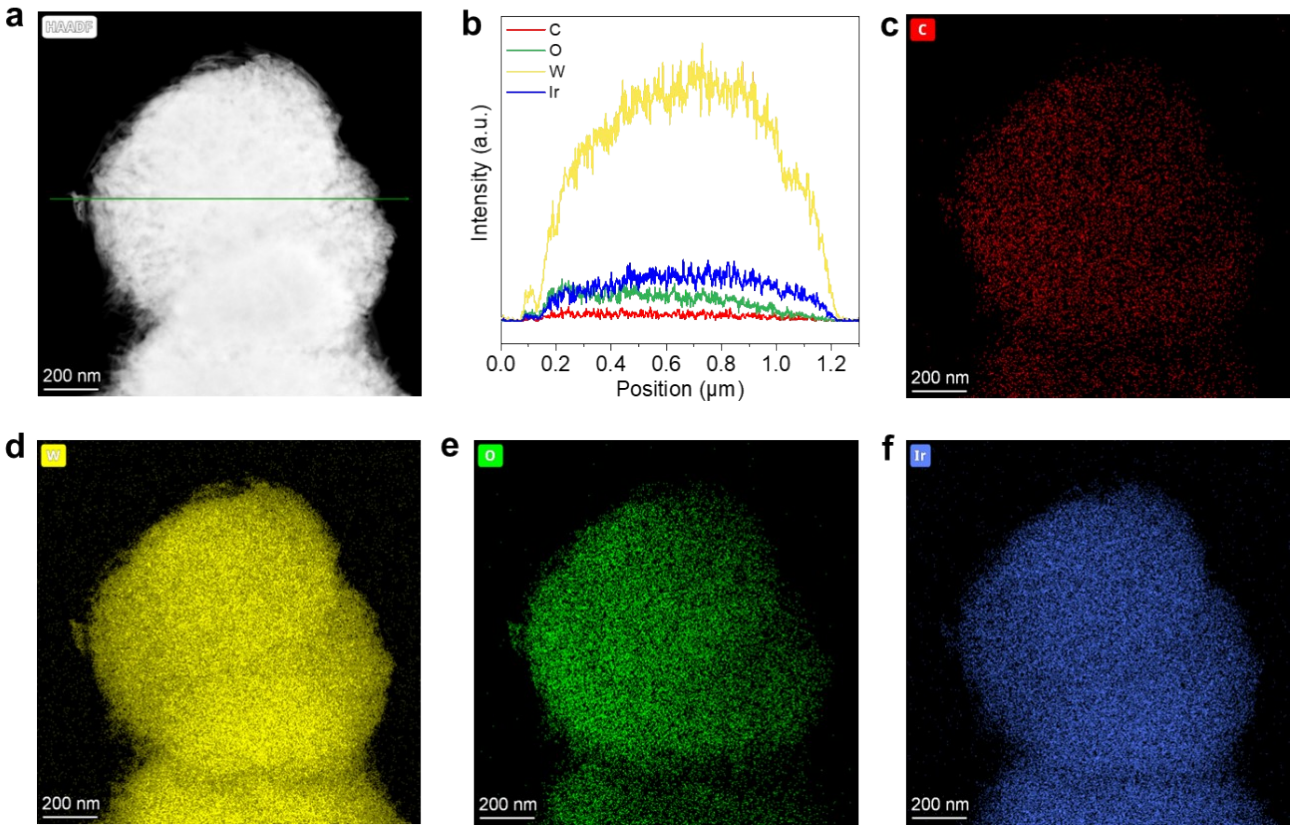

Fig. S5. The HAADF-STEM image (a), line scan (b), and corresponding EDS mappings (c-f) of Ir-WO_{3-x} show the correlation of the C, W, O, and Ir components.

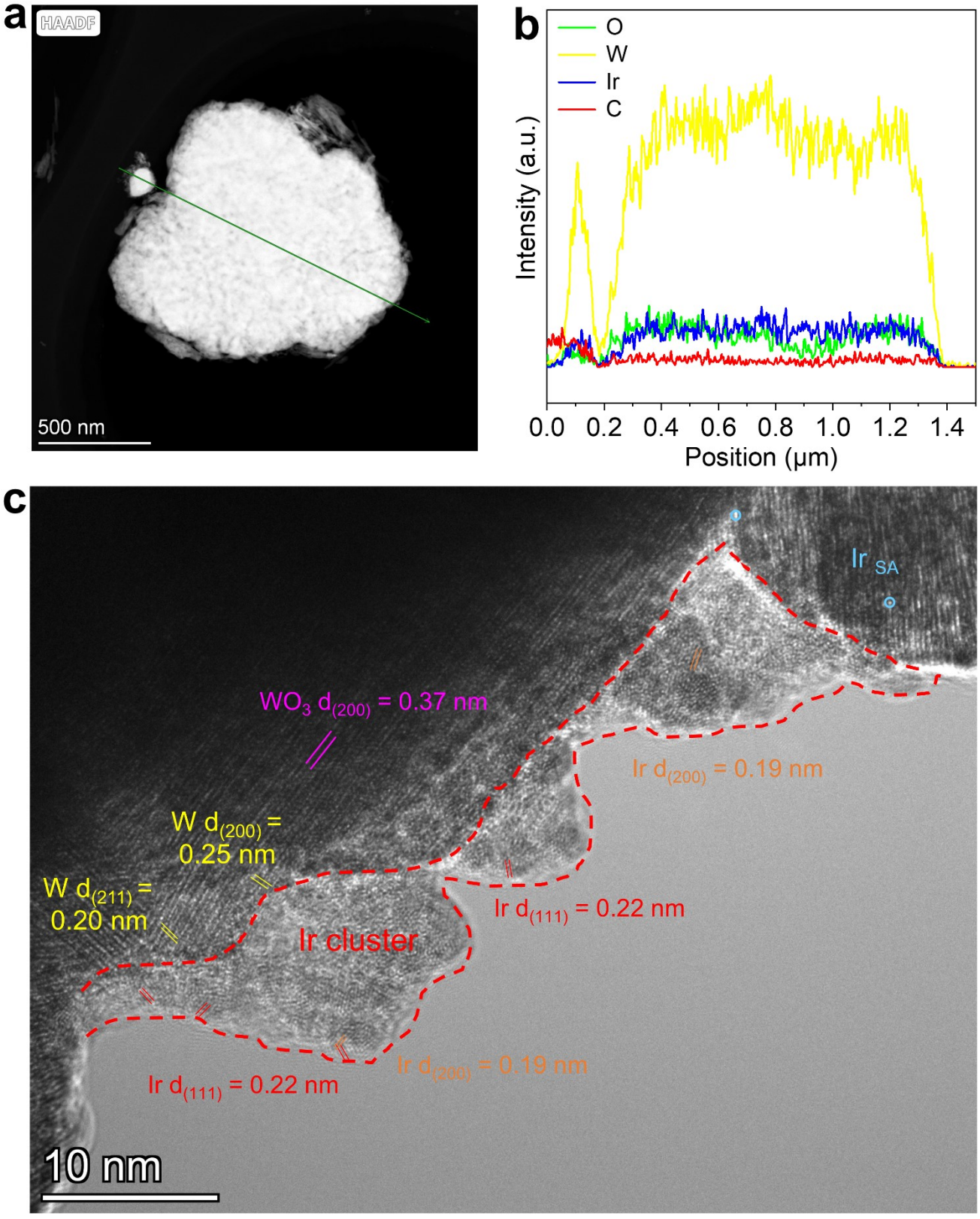

Fig. S6. (a) The HAADF-STEM image of Ir-W/WO_{3-x}. (b) Line scan along the green arow of Ir-W/WO_{3-x} in (a). (c) HRTEM image of Ir-W/WO_{3-x}.

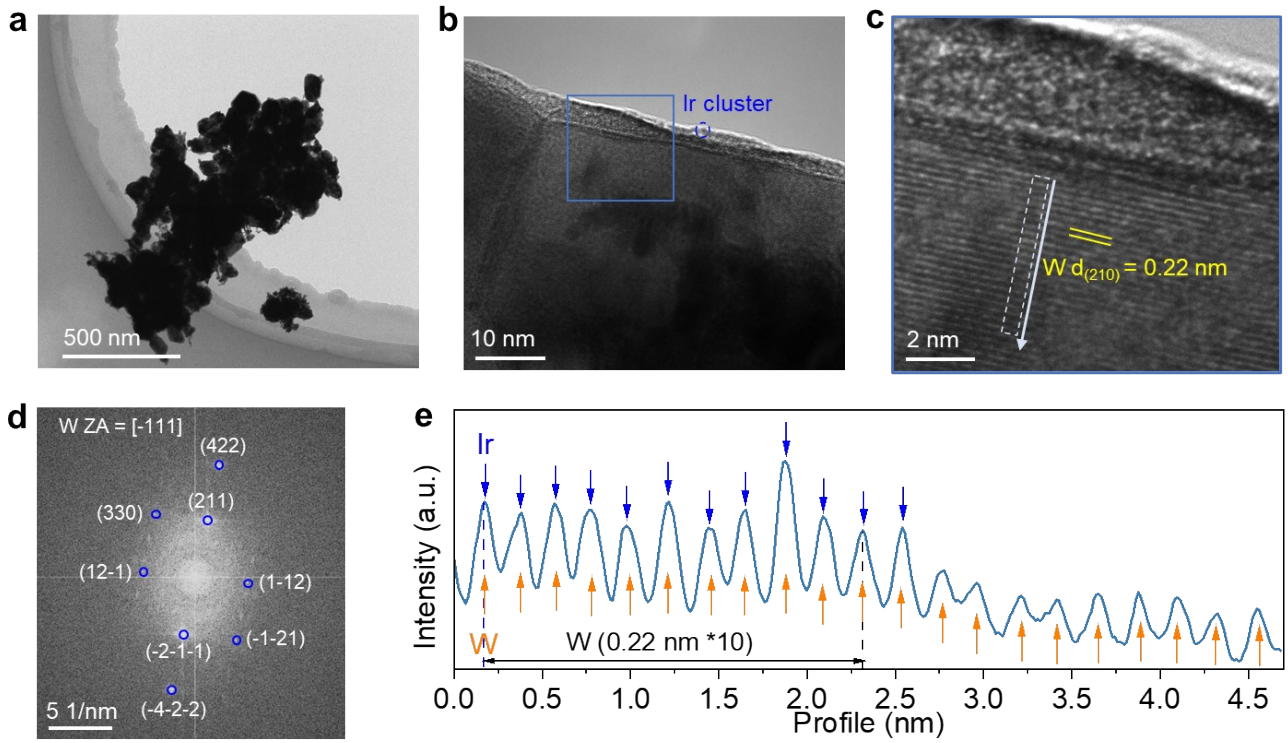

Fig. S7. The TEM image (a) and HRTEM images (b-c) of Ir-W, and corresponding FFT and the corresponding FFT pattern along with the [-111] zone axis. e) The line intensity profiles of the blue dotted area of Ir-W from (c).

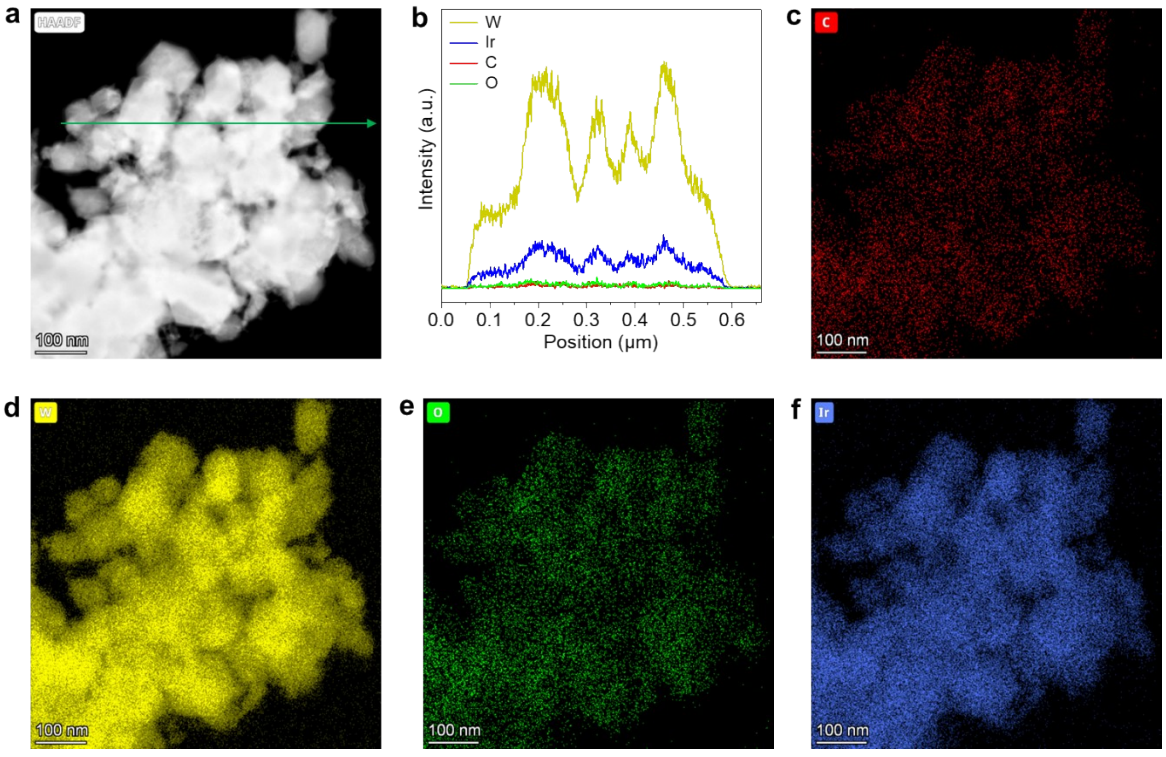

Fig. S8. The HAADF-STEM image (a), line scan (b), and corresponding EDS mappings (c-f) of Ir-W show the correlation of the C, W, O, and Ir components.

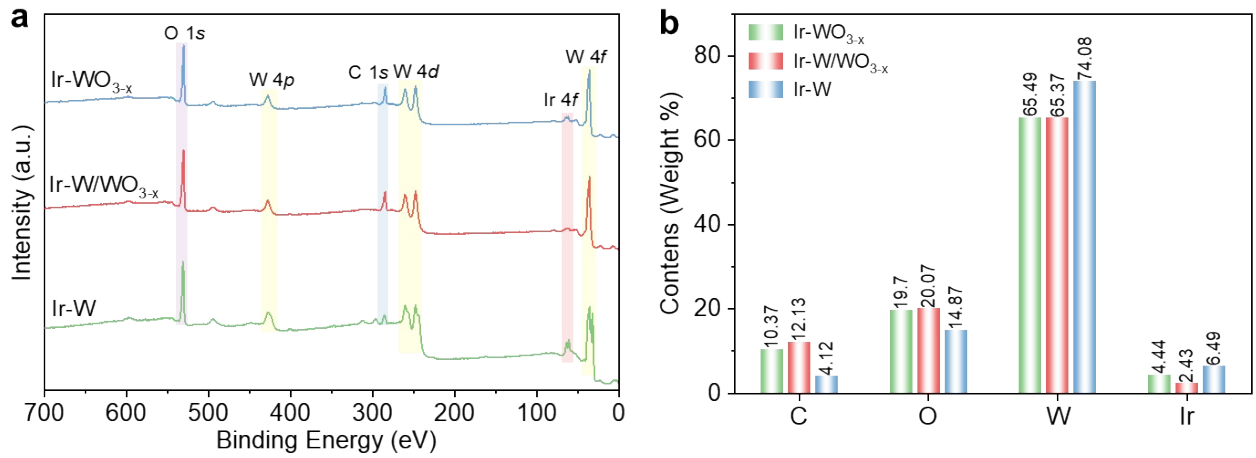

Fig. S9. (a) XPS survey spectra, and (b) atom ratios of Ir-WO_{3-x}, Ir-W/WO_{3-x}, and Ir-W.

Table S1. Surface atomic and weight ratios of catalysts that are determined by XPS.

Catalysts	**C (At%)**	**O (At%)**	**W (At%)**	**Ir (At%)**
Ir-WO_{3-x}	34.89	49.78	14.40	0.93
Ir-W/WO_{3-x}	38.36	47.65	13.51	0.48
Ir-W	20.04	54.30	23.55	2.11
Catalysts	**C (Wt%)**	**O (Wt%)**	**W (Wt%)**	**Ir (Wt%)**
Ir-WO_{3-x}	10.37	19.70	65.49	4.44
Ir-W/WO_{3-x}	12.13	20.07	65.37	2.43
Ir-W	4.12	14.87	74.08	6.94

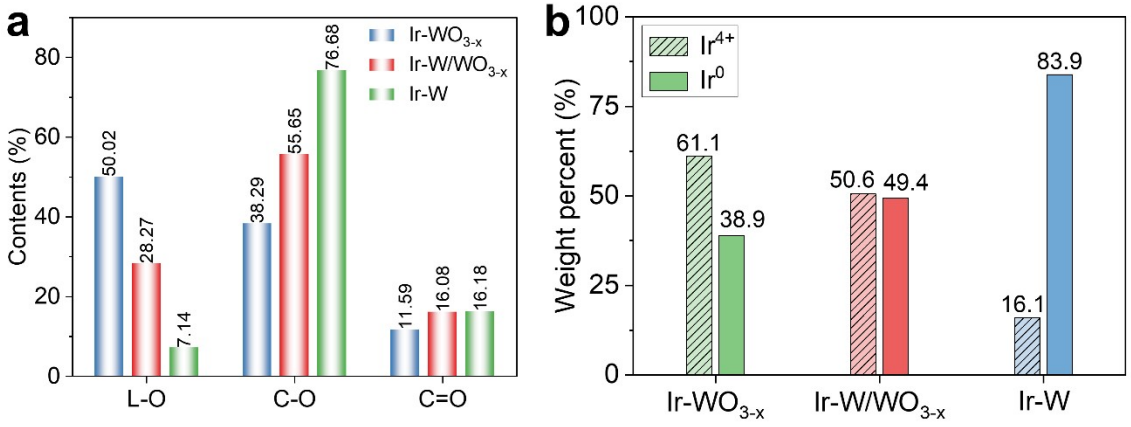

Fig. S10. (a) Oxygen ratios variation of lattice-O (L-O), C-O, C=O, and (b) Ir^{4+} and Ir^{0} species in Ir-WO_{3-x}, Ir-W/WO_{3-x}, and Ir-W that are determined by XPS, respectively.

Table S2. Surface oxygen ratios of metal-O (M-O), C-O, and C=O in catalysts that are determined by XPS.

Catalysts	M-O (%)	C-O (%)	C=O %)
Ir-WO_{3-x}	56.50	34.66	8.34
Ir-W/WO_{3-x}	47.40	38.27	14.33
Ir-W	25.23	63.82	10.95

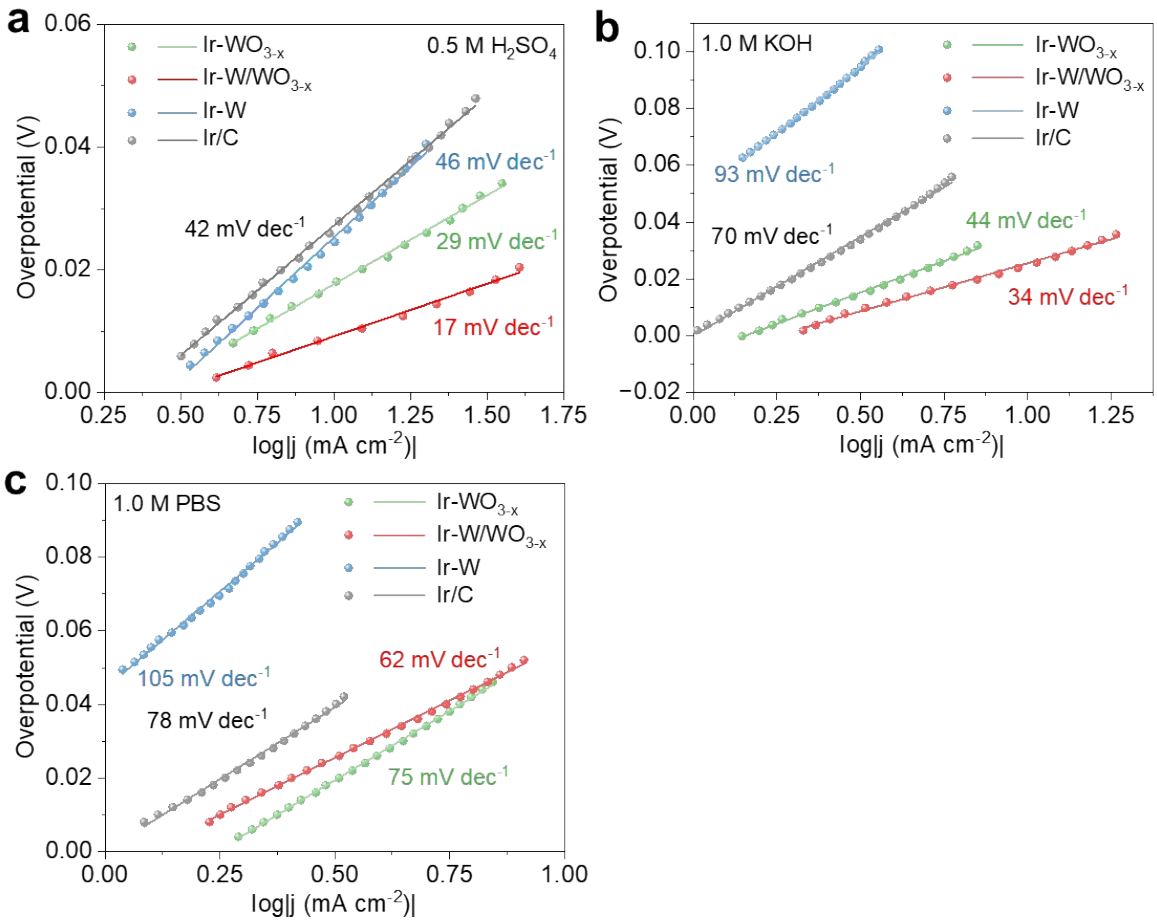

Fig. S11. The HER Tafel slopes of Ir-WO_{3-x}, Ir-W/WO_{3-x}, Ir-W, and Ir/C in 0.5 M H_2SO_4 (a), 1.0 M PBS (b), and 1.0 M KOH (c), respectively.

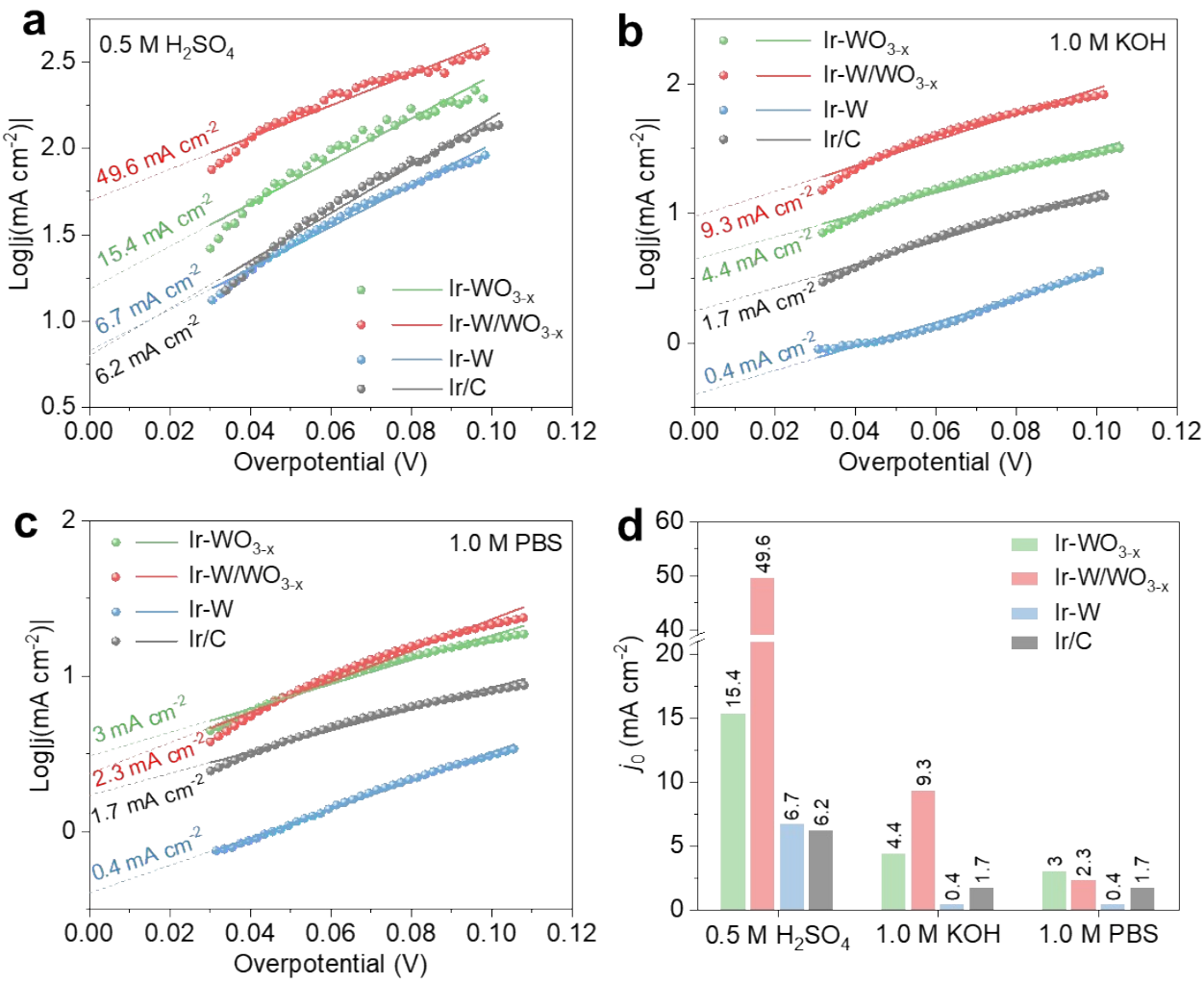

Fig. S12. The HER exchange current density (j_0) of Ir-WO_{3-x}, Ir-W/WO_{3-x}, Ir-W, and Ir/C in (a) 0.5 M H_2SO_4, (b) 1.0 M KOH, and (c) 1.0 M PBS. (d) The comparison of j_0 values for different catalysts.

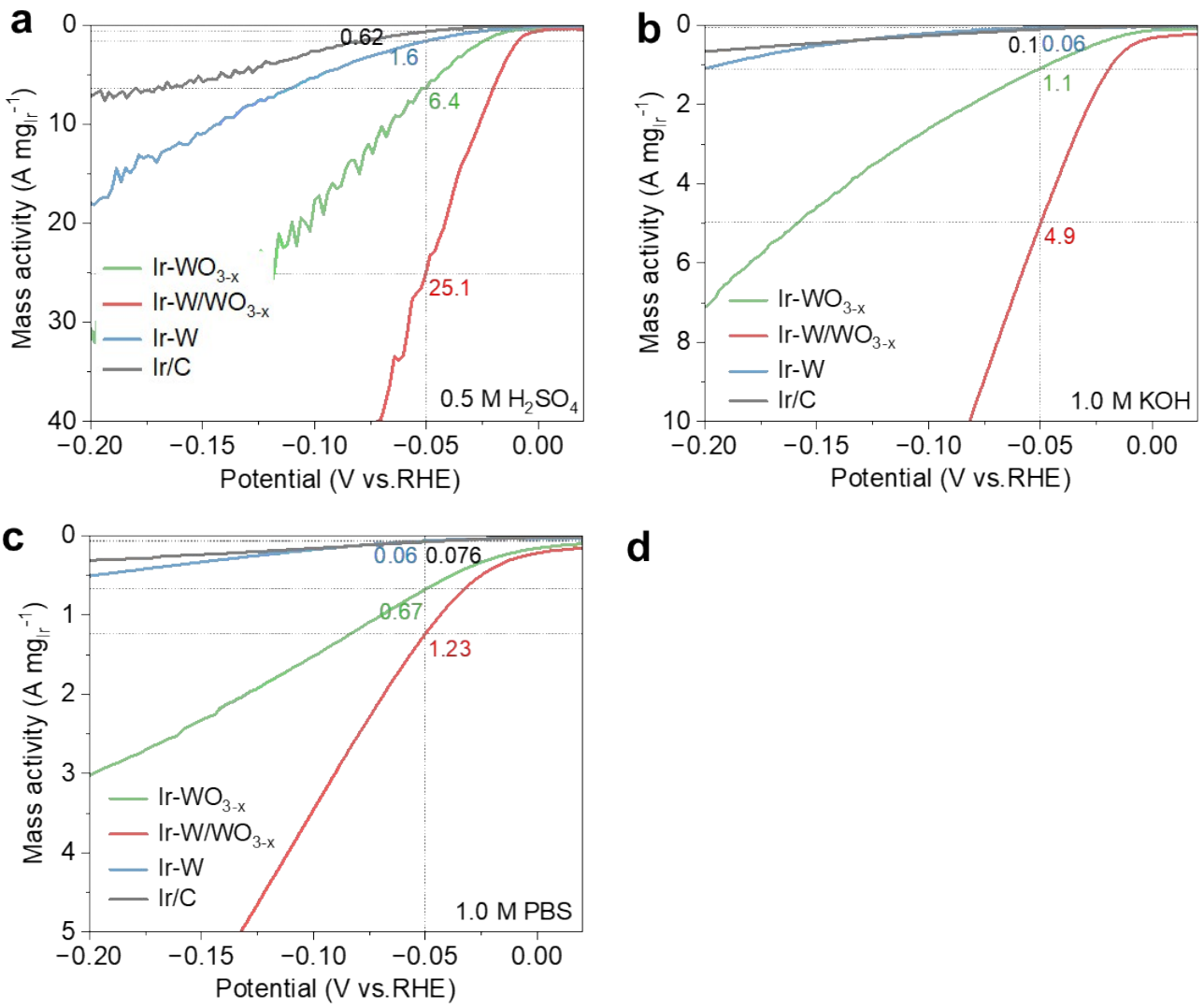

Fig. S13. Mass activity curves of catalysts based on the weight content of Ir in (a) 0.5 M H_2SO_4, (b) 1.0 M KOH, and (c) 1.0 M PBS for HER.

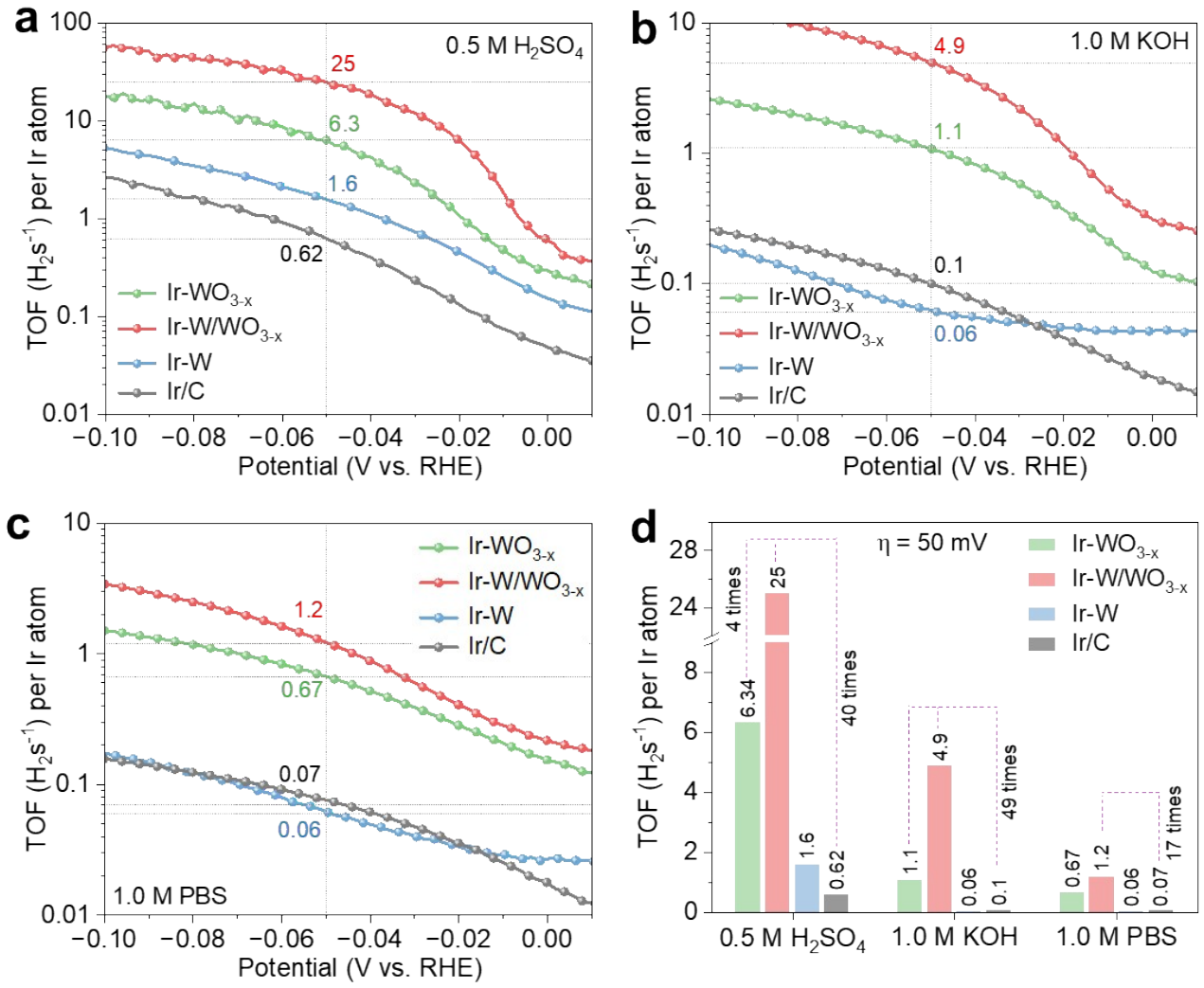

Fig. S14. The calculated HER TOF values of Ir-WO_{3-x}, Ir-W/WO_{3-x}, Ir-W, and Ir/C based on Ir atoms in (a) 0.5 M H_2SO_4, (b) 1.0 M KOH, and (c) 1.0 M PBS. (d) The comparison of TOF values at the overpotential of 50 mV for different catalysts.

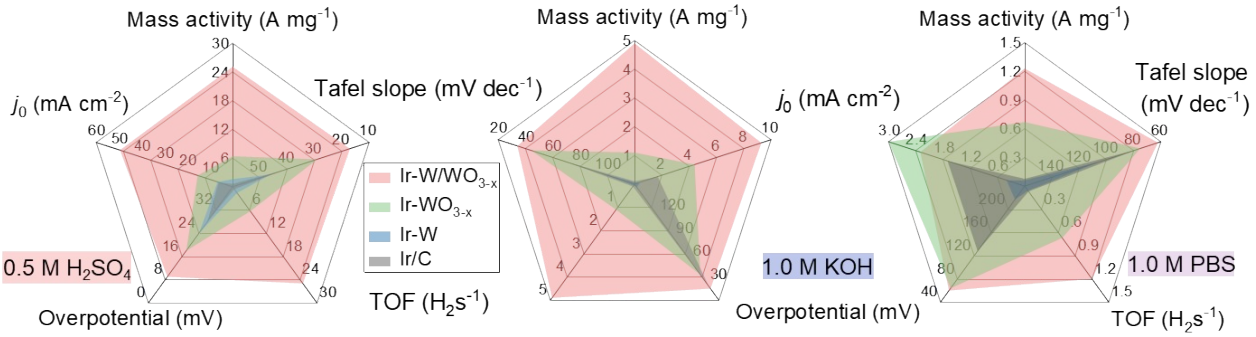

Fig. S15. Performance comparison on the mass activities, Tafel slopes, TOF, overpotential, and j_0 of catalysts in different electrolytes.

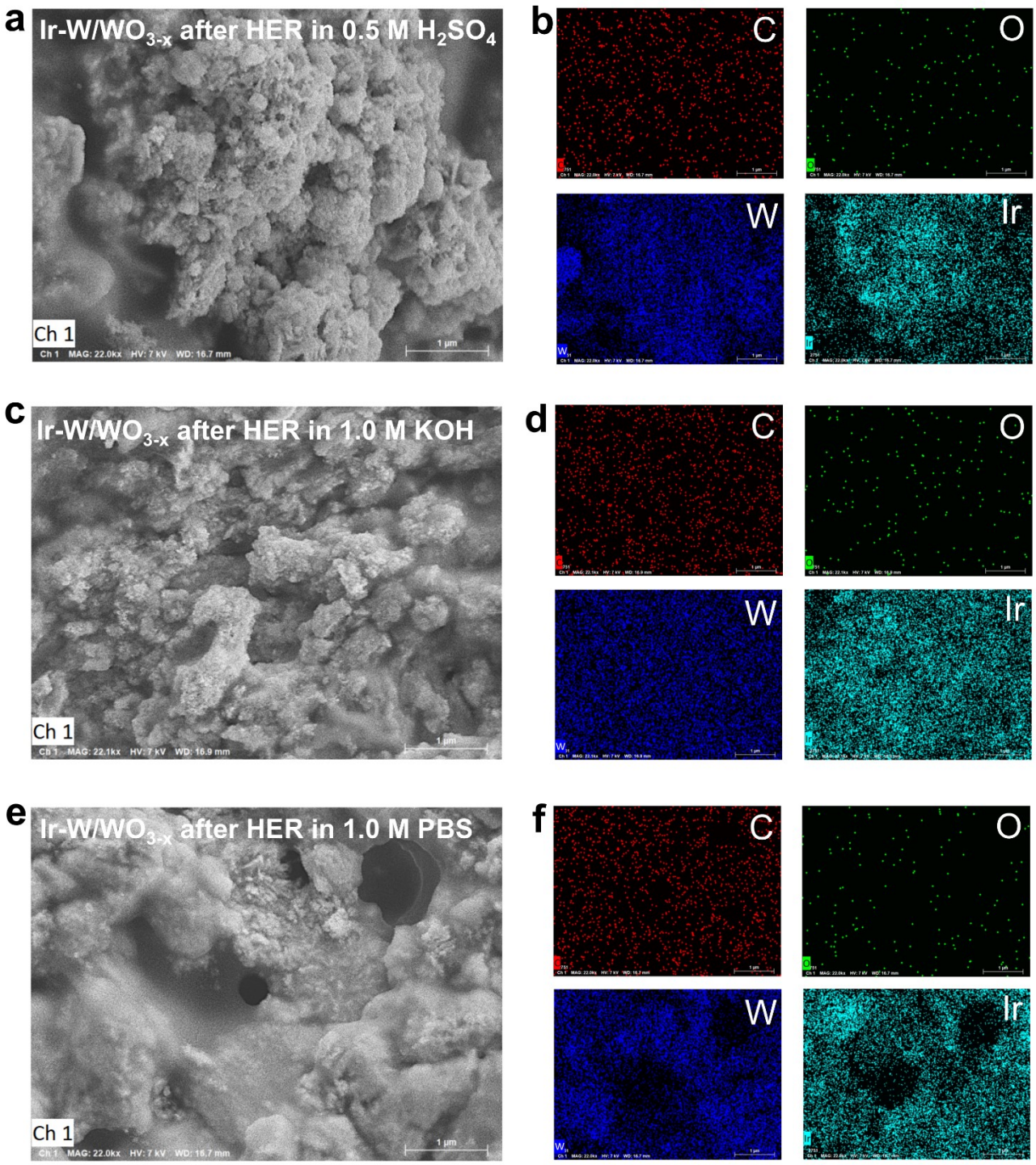

Fig. S16. The SEM images and corresponding EDS mapping of Ir-W/WO_{3-x}/CC after HER stability test in (a, b) 0.5 M H_2SO_4, (c, d) 1.0 M KOH, and (e, f) 1.0 M PBS.

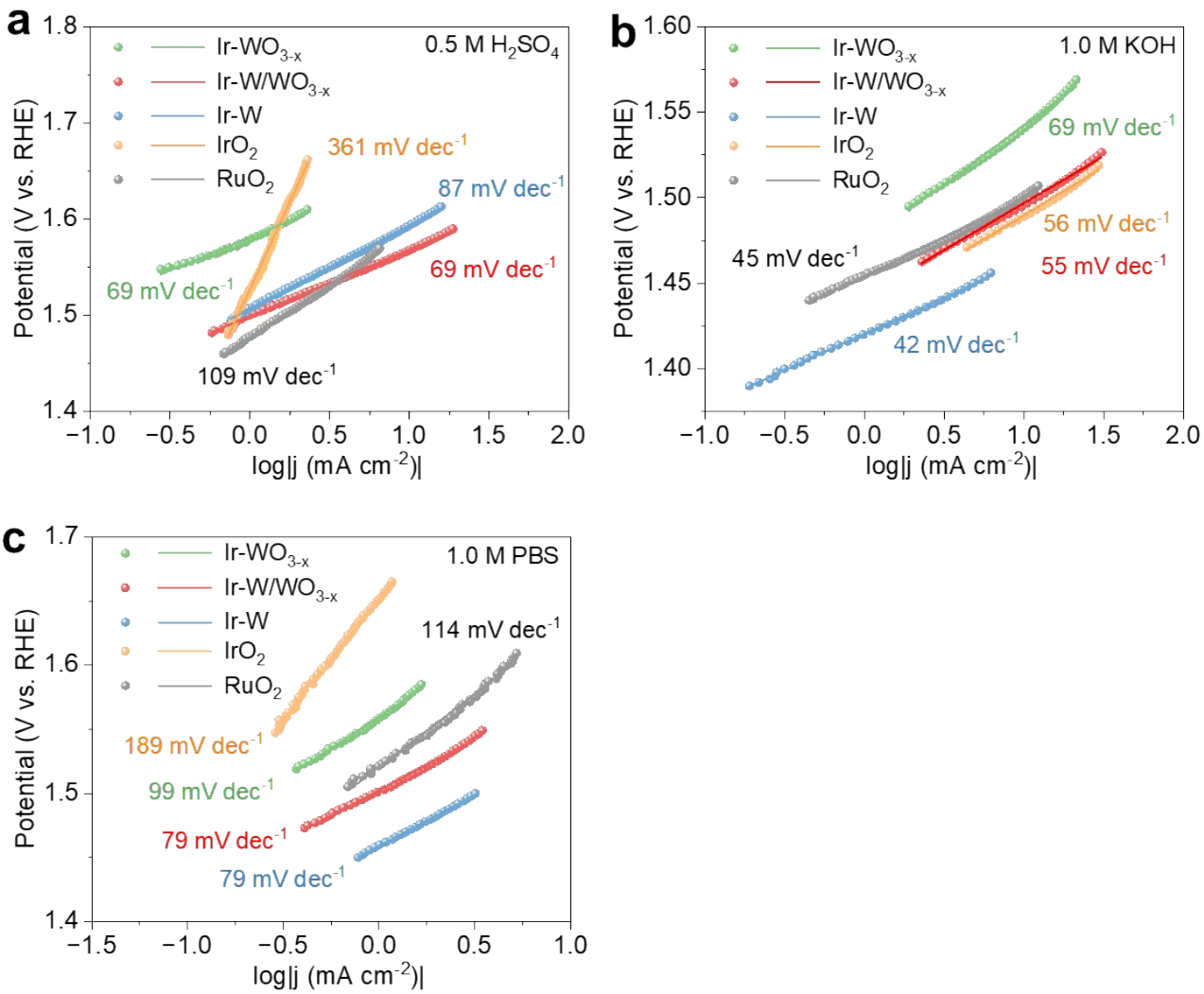

Fig. S17. The OER Tafel slopes of Ir-WO_{3-x}, Ir-W/WO_{3-x}, Ir-W, IrO_2, and RuO_2 in 0.5 M H_2SO_4 (a), 1.0 M PBS (b), and 1.0 M KOH (c), respectively.

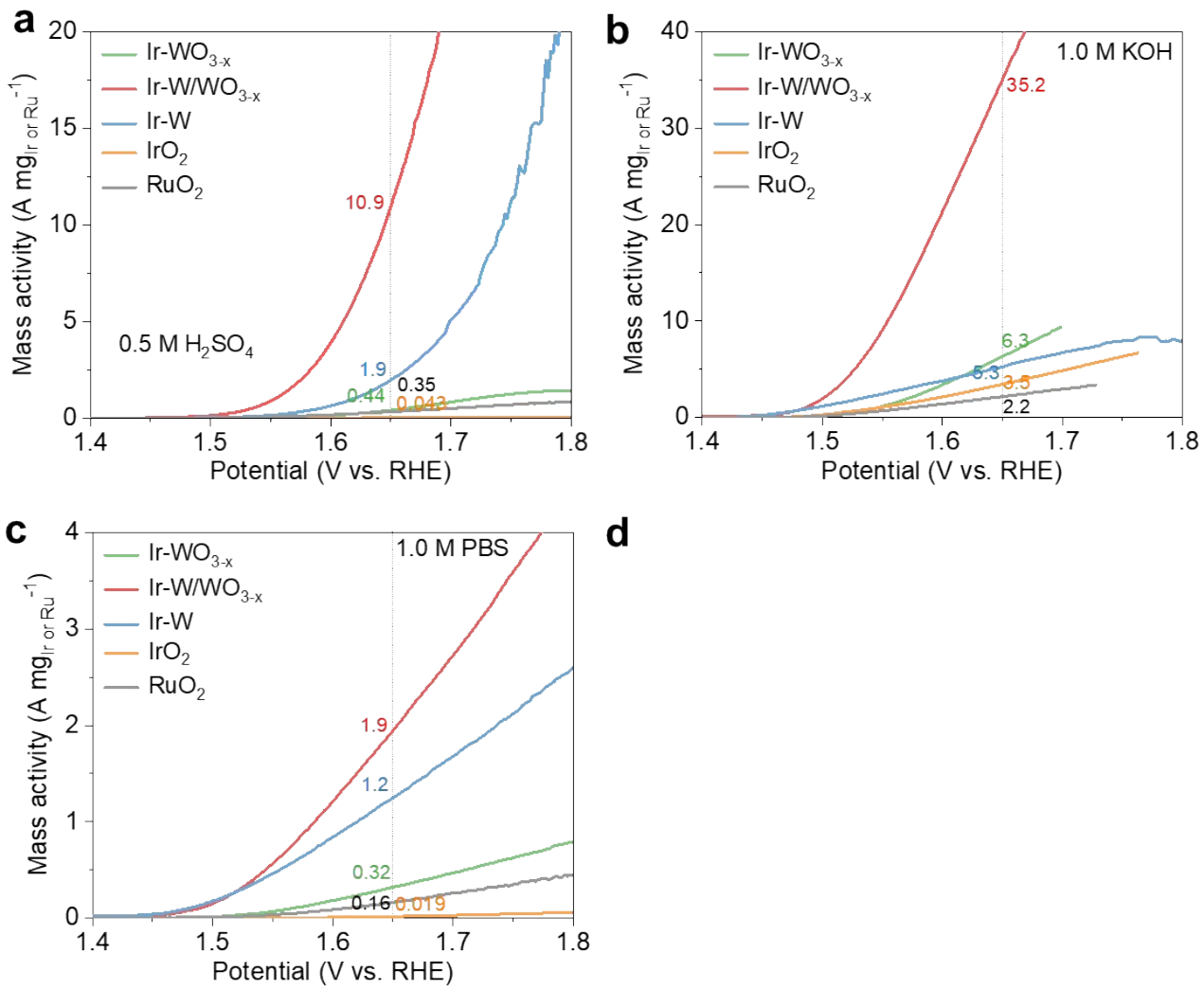

Fig. S18. Mass activity curves of catalysts based on the weight content of Ir or Ru in (a) 0.5 M H_2SO_4, (b) 1.0 M KOH, and (c) 1.0 M PBS for OER.

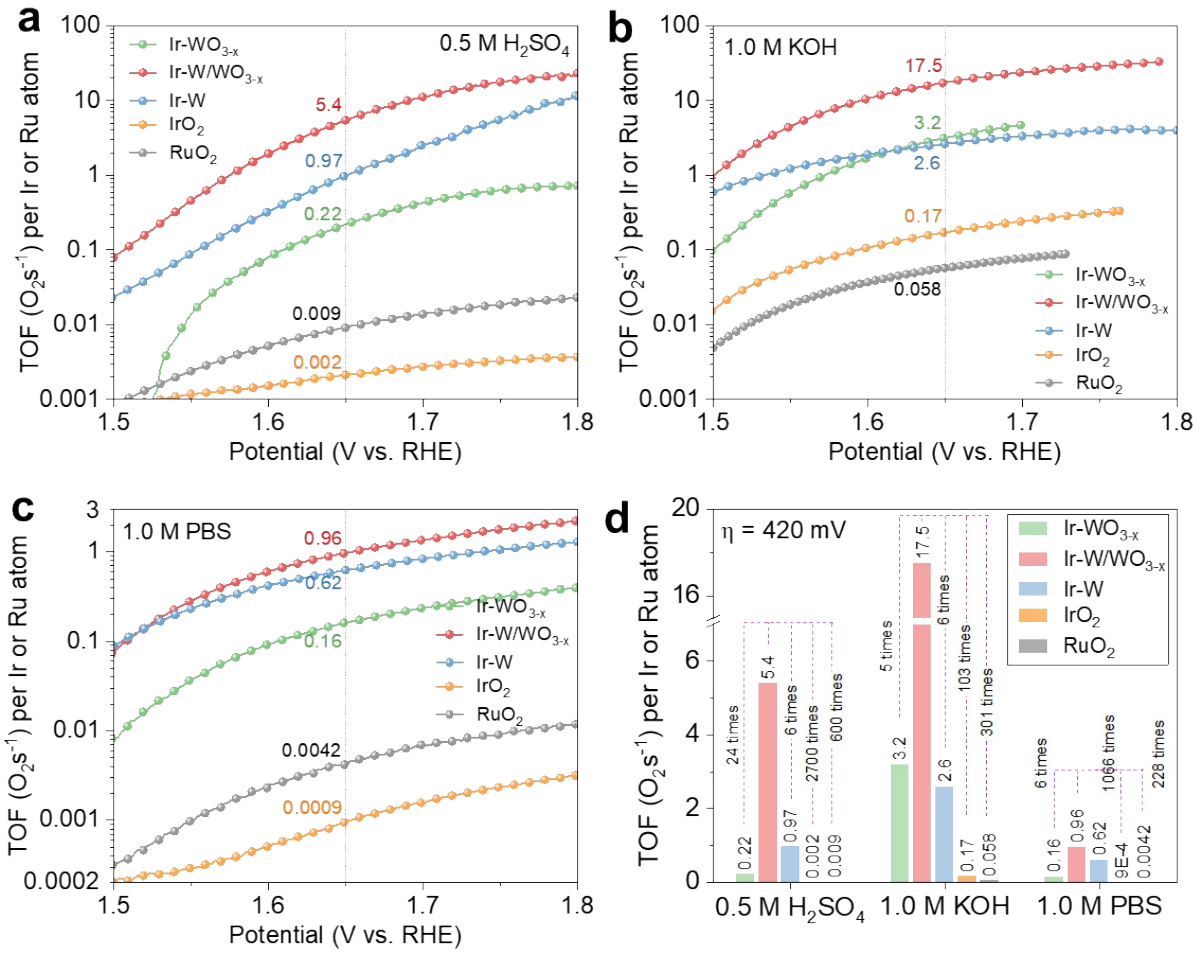

Fig. S19. The calculated OER TOF values of Ir-WO_{3-x}, Ir-W/WO_{3-x}, Ir-W, IrO_2, and RuO_2 based on Ir or Ru atoms in (a) 0.5 M H_2SO_4, (b) 1.0 M KOH, and (c) 1.0 M PBS. (d) The comparison of TOF values at the overpotential of 420 mV for different catalysts.

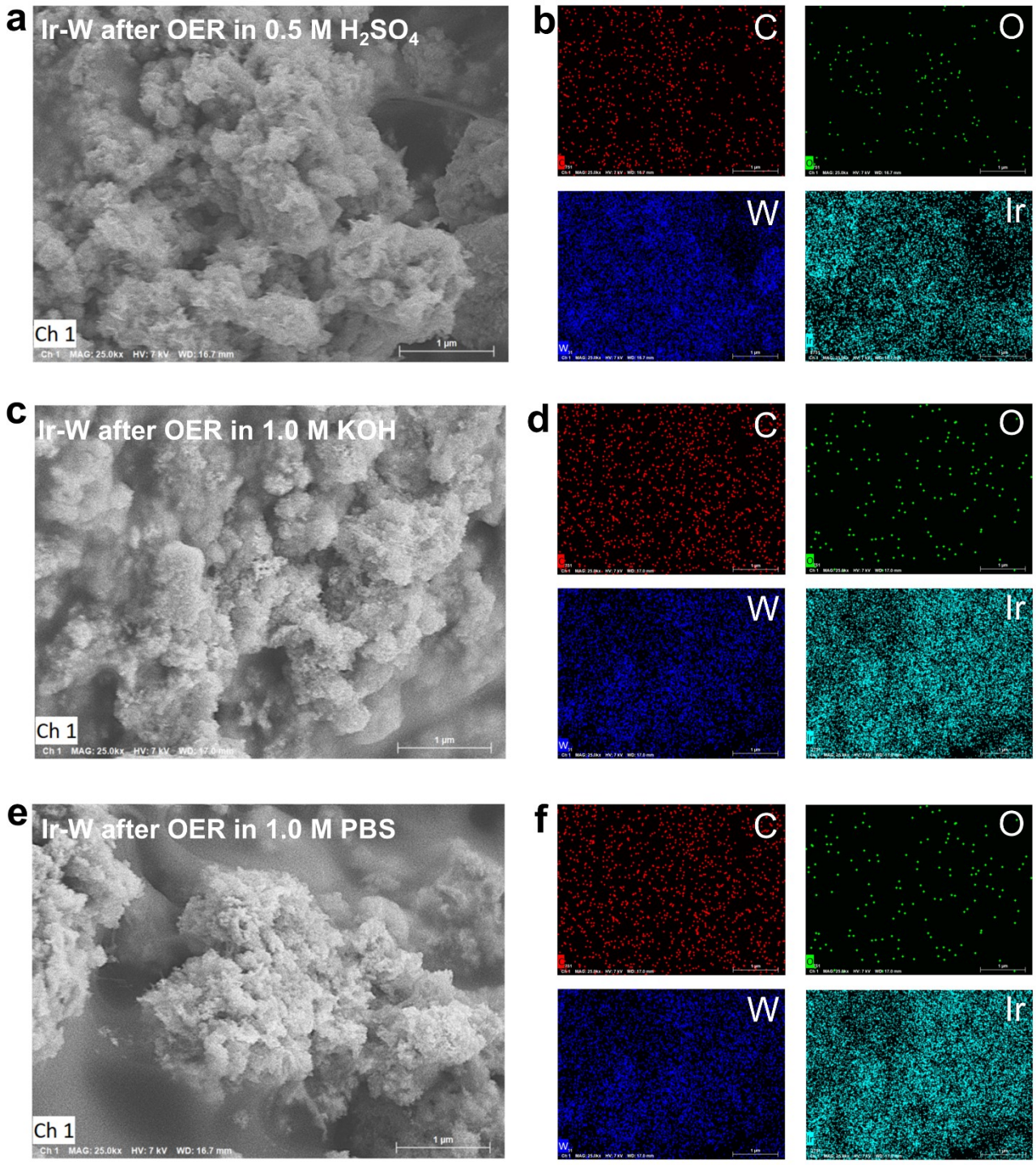

Fig. S20. The SEM images and corresponding EDS mapping of Ir-W/CC after OER stability test in (a, b) 0.5 M H_2SO_4, (c, d) 1.0 M KOH, and (e, f) 1.0 M PBS.

Table S3. Performance comparison of Ir-W/WO_{3-x} || Ir-W with other recently reported catalysts for water splitting in 1.0 M PBS.

Catalysts	OWS (V)/*j* (mA cm^{-2})	Reference
Ir-W || Ir-W	1.593/10	This work
CoMoNiS-NF-31 || CoMoNiS-NF-31	1.8/10	[1]
3D CoBOx/NiSe ||3D CoBOx/NiSe	1.8/10	[2]
Mn-doped FeP/$Co_3(PO_4)_2$ || Mn-doped FeP/$Co_3(PO_4)_2$	1.82/10	[3]
Fe@Fe_xNiO/Ni@Ni_yCoP||Fe@Fe_xNiO/Ni@Ni_yCoP	1.86/10	[4]
$Ni(S_{0.5}Se_{0.5})_2$ || $Ni(S_{0.5}Se_{0.5})_2$	1.87/10	[5]
$Ni_{0.1}Co_{0.9}$P-CFP || $Ni_{0.1}Co_{0.9}$P-CFP	1.89/10	[6]
S-$NiFe_2O_4$/NF || S-$NiFe_2O_4$/NF	1.95/10	[7]

1. Y. Yang, H. Yao, Z. Yu, S. M. Islam, H. He, M. Yuan, Y. Yue, K. Xu, W. Hao, G. Sun, H. Li, S. Ma, P. Zapol and M. G. Kanatzidis, *J. Am. Chem. Soc.* , 2019, **141**, 10417-10430.
2. Y. Liu, T. Sakthivel, F. Hu, Y. Tian, D. Wu, E. H. Ang, H. Liu, S. Guo, S. Peng and Z. Dai, *Adv. Energy Mater.*, 2023, **13**, 2203797.
3. H. Liu, X. Peng, X. Liu, G. Qi and J. Luo, *ChemSusChem*, 2019, **12**, 1334-1341.
4. Q. Che, X. Zhou, Q. Liu, Y. Tan and Q. Li, *J. Mater. Chem. A*, 2021, **9**, 5833-5847.
5. L. Zeng, K. Sun, Y. Chen, Z. Liu, Y. Chen, Y. Pan, R. Zhao, Y. Liu and C. Liu, *J. Mater. Chem. A*, 2019, **7**, 16793-16802.
6. R. Wu, B. Xiao, Q. Gao, Y. R. Zheng, X. S. Zheng, J. F. Zhu, M. R. Gao and S. H. Yu, *Angew. Chem. Int. Ed.*, 2018, **57**, 15445-15449.
7. J. Liu, D. Zhu, T. Ling, A. Vasileff and S.-Z. Qiao, *Nano Energy*, 2017, **40**, 264-273.